JOURNAL OF NANOMATERIALS AND APPLICATIONS

Journal of Nanomaterials and Applications

Journal homepage: https://jna.com.vn

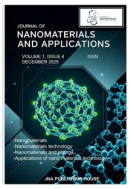

Comparative assessment of exchange-correlation functionals for structural, electronic, and optical properties of rhombohedral $Bi_{0.5}Na_{0.5}TiO_3$

Le Minh Thu [1], Nguyen Phuong Thao [2], Duong Quoc Van [3,*]

[1,2,3] Faculty of Physics, Hanoi National University of Education, 136 Xuan Thuy, Cau Giay, 100000, Ha Noi, Viet Nam.

Article info

Type of articles:
Original research paper

Corresponding author*:
Duong Quoc Van:
vandq@hnue.edu.vn

Received: 12 July 2026
Revised: 03 August 2026
Accepted: 09 August 2026
Published: 28 August 2026

Abstract: A systematic first-principles investigation was performed to evaluate the performance of LDA and various GGA functionals (PBE, RPBE, PBESol, PW91, WC) on the structural, electronic, and optical properties of rhombohedral $Bi_{0.5}Na_{0.5}TiO_3$(BNT). The results reveal that while PBESol and WC yield superior lattice parameters, GGA-PBE and GGA-PW91 provide the most consistent overall description of structural properties, direct bandgap energies, and optical absorption spectra. LDA severely underestimates lattice constants and bandgaps, whereas RPBE overestimates lattice parameters. Analysis of partial density of states indicates that the valence band is dominated by O-2p and Ti-3d hybridization, while the conduction band mainly consists of Ti-3d and Bi-6p states. Overall, GGA-PBE emerges as the most reliable functional for studying pristine and modified BNT-based materials.

Keywords: BNT, DFT, ab-initio calculation, exchange-correlation functionals, comparison

1. Introduction

$Bi_{0.5}Na_{0.5}TiO_3$ (BNT) is one of the most promising lead-free ferroelectric materials for replacing conventional Pb-based piezoelectric ceramics because of its excellent ferroelectric, dielectric, and piezoelectric properties together with its environmentally friendly composition . Since its first discovery by Smolenskii and Agranovskaya in the early 1960s [1], BNT has attracted considerable attention for applications in sensors, actuators, energy harvesting devices, and non-volatile ferroelectric memories due to its relatively large remanent polarization, high Curie temperature, and good thermal stability [2].

Depending on temperature, BNT exhibits three crystallographic phases: a rhombohedral phase (space group R3c) below approximately 500 K, a tetragonal phase at intermediate temperatures, and a cubic paraelectric phase above about 800 K [3-5]. Among these phases, the rhombohedral structure is the most technologically important because it possesses spontaneous ferroelectric polarization and piezoelectric activity. Experimental studies have reported a remanent polarization of approximately 38 $\mu C.cm^{-2}$ and a coercive field around 73 $kV.\ cm^{-1}$ for rhombohedral BNT, making it one of the representative lead-free ferroelectric perovskites [6]. Although its piezoelectric coefficient is lower than those of commercial $Pb(Zr,Ti)O_3$ (PZT)-based ceramics, BNT has become an attractive alternative owing to increasingly stringent environmental regulations restricting the use of lead-containing electronic materials. Consequently, extensive efforts have been devoted to improving its physical properties through chemical substitution, defect engineering, and solid-solution formation [7-9].

In parallel with experimental developments, first-principles calculations based on density functional theory (DFT) have become indispensable tools for understanding the microscopic origin of the structural, electronic, optical, and magnetic properties of BNT. Compared with experimental approaches, DFT calculations provide detailed information about the electronic structure, chemical bonding, density of states, and charge distribution at the atomic scale while requiring significantly lower cost and time [10]. Moreover, computational studies allow researchers to predict the effects of dopants, defects, and structural distortions before experimental synthesis, thereby accelerating the development of new BNT-based functional materials [11].

Numerous DFT investigations have been performed on BNT using different computational packages, including CASTEP [12, 13], VASP [14, 15] and WIEN2k [16, 17]. Previous studies consistently demonstrated that rhombohedral BNT is a semiconductor with a direct band gap and that the valence band is mainly composed of O-2p states hybridized with Ti-3d orbitals, whereas the conduction band is dominated by Ti-3d and Bi-6p states [18]. Other theoretical works have investigated the lattice dynamics, elastic behavior, optical response, and magnetic properties of doped BNT systems [19-21]. These studies have significantly improved the understanding of BNT and provided valuable guidance for experimental research.

However, despite the extensive application of DFT to BNT, there is still no consensus regarding the most suitable exchange-correlation functional for accurately describing its physical properties. Different studies have employed various local density approximation (LDA) and generalized gradient approximation (GGA) functionals, often leading to inconsistent predictions of lattice parameters, total energies, electronic band gaps, and optical properties. For example, some investigations suggested that LDA provides satisfactory structural optimization, whereas others reported that GGA-based functionals, such as PBE or PBESol, yield better agreement with experimental measurements [22]. Since the exchange-correlation functional represents the largest approximation in conventional DFT calculations, its selection directly influences the reliability of theoretical predictions, particularly for complex oxide perovskites such as BNT [23]. Therefore, a systematic comparison of commonly used functionals under identical computational conditions is highly desirable but remains relatively limited in the literature.

Such a comparative study is particularly important because BNT serves as the parent compound for a wide variety of modified materials obtained through substitution of transition-metal ions or alkaline-earth elements [20, 24]. Reliable prediction of the structural stability, electronic structure, magnetic behavior, and optical response of these modified systems strongly depends on the choice of exchange-correlation functional [23, 25]. An inappropriate functional may introduce significant errors that propagate into subsequent investigations of doped BNT materials, making the interpretation of experimental observations more difficult.

The electronic properties of rhombohedral BNT are strongly influenced by several structural factors. First, the rhombohedral distortion (space group R3c) induces TiO_6 octahedral tilting and off-center displacements of Bi^{3+}, Na^{+}, and Ti^{4+}, which modify the overlap between Ti-3d, O-2p, and Bi-6p orbitals [18, 20]. Second, the stereochemically active Bi $6s^2$ lone-pair electrons produce strong Bi–O hybridization, enhancing ferroelectric polarization and affecting the valence-band dispersion [17, 26]. Third, intrinsic defects such as oxygen vacancies and cation disorder may introduce localized electronic states within the band gap [21, 27]. Finally, the predicted electronic structure also depends on the choice of exchange-correlation functional because different functionals describe electron localization and exchange interactions with different accuracy.

In the present work, we perform a comprehensive first-principles investigation of rhombohedral $Bi_{0.5}Na_{0.5}TiO_3$ using six widely adopted exchange-correlation functionals, including the LDA-PZ functional and five GGA functionals (PBE, RPBE, PBESol, PW91, and WC), implemented within the CASTEP package. Their performances are systematically evaluated by comparing the optimized lattice constants, total energies, electronic band structures, density of states, spin characteristics, and optical absorption spectra with available experimental data. Based on these comparisons, we identify the most reliable functional for accurately describing the structural and electronic properties of BNT, thereby providing a practical guideline for future first-principles studies of pristine and chemically modified BNT-based materials.

In this research, we investigate the influence of functionals on the structural, electronic and optical properties of BNT in order to find out the capable one for ab-initio calculations on further behaviors of BNT and BNT-based materials.

2. Computational Methods

The initial unit cell of BNT rhombohedral is obtained from experimental result [4], the corresponding lattice constants are a = b = 5.4887 Å and c = 13.5048 Å, as shown in Figure 1. Each unit cell contains a total of number of 30 atom: 3 Bi atoms, 3 Na atoms, 6 Ti atoms and 18 O atoms.

Cambridge Serial Total Energy Package (CASTEP) [28] package, embedded within Material Studio software, was used to investigate the influence of pseudopotentials on the properties of BNT. Both Local Density Approximation (LDA) and Generalized Gradient Approximation (GGA) was used for exchange and correlation effects in materials due to their availability in various calculation softwares.

Perdew-Zunger's (PZ) parametrization [29] of Ceperley-Alder correlation potential [30] was applied for the Local Density Approximation (LDA) calculations. For the Generalized Gradient Approximation (GGA), five different exchange-correlation functionals were systematically investigated: Perdew-Burke-Ernzerhof (PBE) [31], Revised PBE (RPBE) [32], PBE for solids (PBESol) [33], Perdew-Wang 1991 (PW91) [34], and Wu-Cohen (WC) [35].

Electronic wave functions were expanded in a plane-wave basis set with a kinetic energy cutoff of 550 eV, which was determined after rigorous total-energy convergence tests (energy change < $1.0.10^{-6}$eV/atom). The interactions between valence electrons and ionic cores were described by Ultra Soft Pseudopotentials (USPP) [36]. The valence electron configurations considered in the calculations were Bi: $6s^2\ 5d^{10}\ 6p^3$, Na: $2s^2\ 2p^6\ 3s^1$, Ti: $3s^2\ 3p^6\ 3d^2\ 4s^2$, and O: $2s^2\ 2p^4$.

Brillouin zone integration was performed using Monkhorst-Pack k-point grids. A k-point sampling mesh of 4×4×2 (corresponding to a grid spacing of less than 0.03 $Å^{-1}$) was employed for structural optimization and electronic properties, while a denser k-point mesh of 6×6×3 was utilized for density of states (DOS) and optical calculations. Geometry optimizations were carried out using the Broyden-Fletcher-Goldfarb-Shanno (BFGS) algorithm [37-40]. The convergence thresholds for geometry relaxation were set to: total

energy change < $5.0.10^{-6}$ eV/atom, maximum ionic force < 0.01 eV/Å, maximum stress < 0.02 GPa, and maximum ionic displacement < $5.0.10^{-4}$ Å.

The Monkhorst-Pack grid size [41] generated in the self-consistent calculation is 6×6×6, the total number of k-points in the Brillouin zone is 38, applying to all calculations.

3. Results and Discussions

3.1 Structural Properties

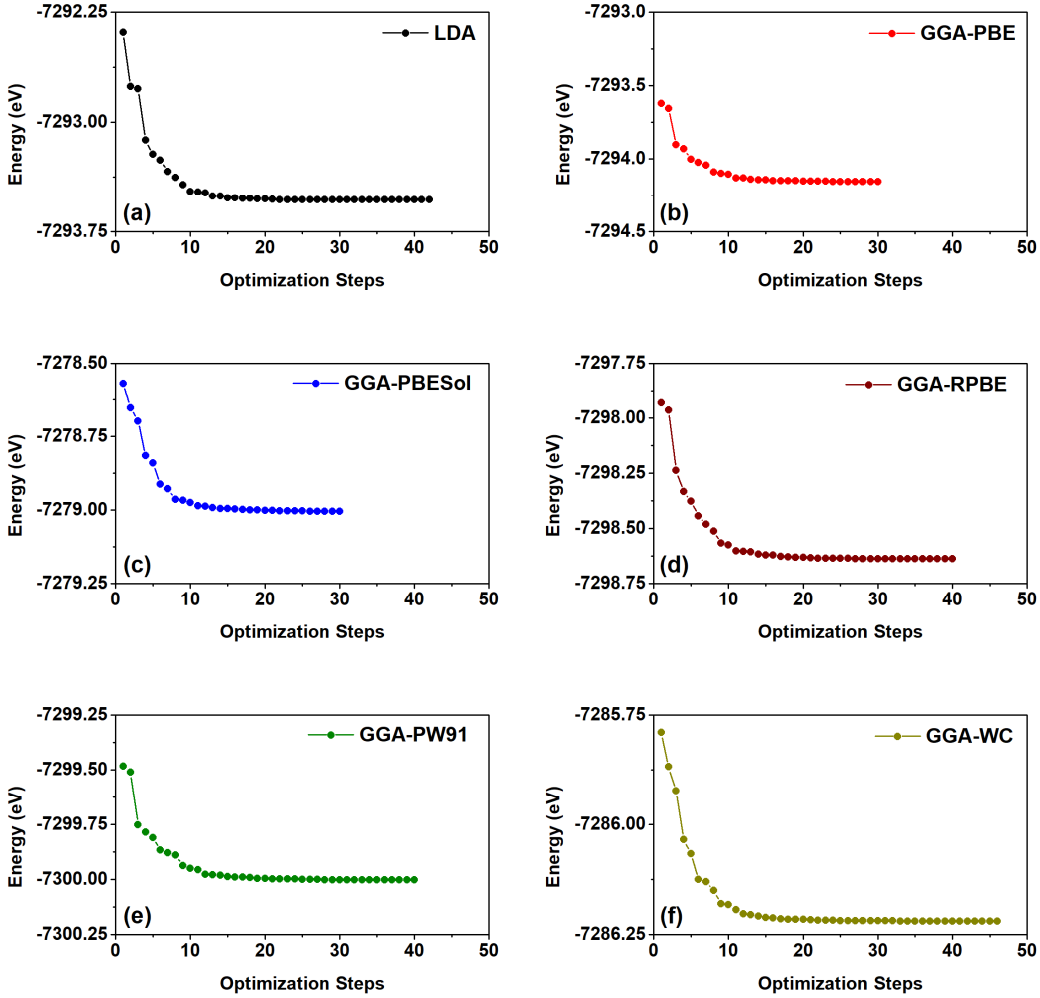

Figure 2. Minimized final energy converges through the optimized iterations of BNT performed by different functionals.

The charts in Figure 2 illustrates the convergence of final energy of BNT unit cells with the optimization steps. Starting with the initial structure, the positions of atoms are adjusted and the total energy of the unit cell is calculated; the process stops when the minimum energy is reached and the stable structure is obtained. It can be seen that after 30 (GGA-PBE and GGA-PBESol) to about 50 steps (GGA-WC), the convergence is achieved and the system has reached an equilibrium state which has minimum total energy. The required steps are different for each functional but the plateau of total energy is reached after about 15 steps. Figure 2 shows that all exchange-correlation functionals converge smoothly toward self-consistent total energies, although the absolute values differ because each functional employs a different exchange-correlation approximation. The lattice constants, relative uncertainties and optimal total energy of BNT obtained via first principle calculation with various

functionals are shown in Table 1. The obtained lattice constants and their relative uncertainties, compared to the experimental values, are shown in Figure 3; the calculated total energies for BNT unit cells are displayed in Figure 4.

Table 1. Calculated structural properties of BNT material.

Parameters	Functionals						
	LDA	PBE	PBESol	RPBE	PW91	WC	Exp [4]
a = b (Å)	5.3622	5.4942	5.4425	5.5419	5.4897	5.4461	5.4887
$\varepsilon_{a,b}$ (%)	2.30	0.10	0.84	0.97	0.02	0.78	0
c (Å)	13.3703	13.8319	13.5422	14.1148	13.8081	13.5435	13.5048
ε_c (%)	0.99	2.42	0.28	4.52	2.25	0.29	0
Total Energy (eV)	-7293.53	-7294.16	-7279.01	-7298.64	-7300.00	-7286.21	

Table 1 reveals that the final structures are in a good agreement with Rietveld neutron powder profile analysis of Jones et al [4]. The rhombohedral structures is unchanged throughout all optimization process with different functionals. LDA functional give total underestimated results with a underestimation of about 2.30% for a and b, 0.99% for c. The highest uncertainty in determination of a and b belongs to LDA with percentage uncertainty of about 2.30% while RPBE pseudopotential give the highest overestimation of c with the relative error of about 4.52%. The PBESol and WC give the best estimations of all three parameters with both relative uncertainties under 1%. Considering that the most important parameters to determine properties of materials are lattice constants, PBESol and WC functionals should be used for prediction of BNT behavior.

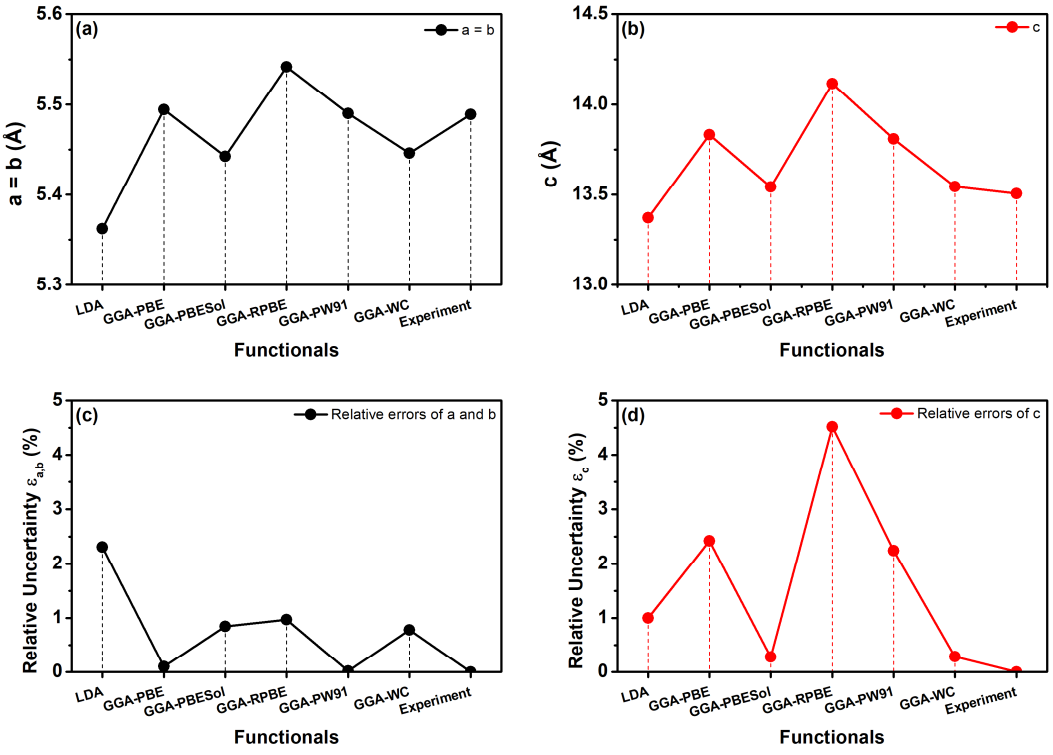

Figure 3. Optimized lattice constants of BNT and relative uncertainties calculated using different functionals.

Physically, the superior accuracy of PBESol and WC functionals in predicting the lattice parameters of rhombohedral BNT stems from their restored gradient expansion for exchange energy. Conventional GGA-PBE overestimates lattice constants due to its soft exchange potential in regions of slowly varying electron densities, which is a known limitation in dense bulk solids. Conversely, LDA over-binds atoms

and underestimates lattice parameters owing to the neglect of density gradients. PBESol and WC modify the second-order gradient expansion coefficient μ to match the jellium surface energy and sub-rhombus limits, thereby properly balancing the short-range exchange and long-range correlation interactions in complex ABO_3 perovskite oxides.

The present results are consistent with previous first-principles studies on BNT, which predominantly employed either LDA or GGA-PBE functionals for structural optimization. However, these studies generally adopted a single exchange-correlation functional rather than performing a systematic comparison. Therefore, the present work extends the existing literature by providing a comprehensive assessment of the performance of several commonly used functionals for rhombohedral BNT. The total energies reported in Table 1 are the converged self-consistent energies obtained using different exchange-correlation functionals. Since each functional employs a different exchange-correlation approximation and pseudopotential, their absolute total energies are referenced to different energy baselines and therefore cannot be directly compared to evaluate structural stability. A rigorous comparison of stability should instead be based on formation energies or energy differences calculated consistently within the same functional. Consequently, the present work uses the total energies only to verify the convergence of geometry optimization rather than to rank the relative stability of different functionals.

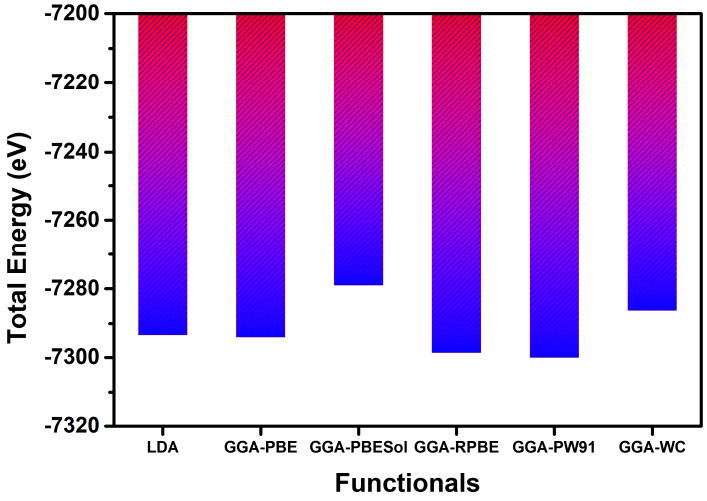

Figure 4. Minimum total energy of BNT calculated using different functionals.

3.2 Electronic Structures

Figure 5 displays the calculated band structures of BNT in the k-path of GFZ, the c electronic bandgaps are listed in Table 2. The results show that BNT is a direct bandgap semiconductor, the lowest energy state in conduction bands (CB) and highest energy state in valence band (VB) located at the center of Brillouin zone or the gamma point (G). It can be seen that the valence bands is in the range of -5 eV to 0 eV while the conduction band take the range of about 2.5 eV to 10 eV. The horizontal lines represents for Fermi level, corresponding energy of 0 eV, stay on the top of valence bands, indicating that BNT behaves as an p-type semiconductor.

Table 2 shows the bandgap values of BNT estimated using different functionals, the experimental results and corresponding relative errors. LDA functional give the lowest bandgap of 2.52 eV, about 18.15% different to the experimental value of 3.08 eV. In contrast, RPBE produced the best estimation of 2.95 eV, which relative error is only 4.35%. The remained functionals can be devided into 2 groups; the

first groups contain PBE and PW91, producing corresponding bandgaps of 2.86 eV and 2.84 eV and relative errors of 7.17 and 7.66%, respectively. The PBESol and WC functionals belongs to the second group with the estimated bandgaps of 2.78 and 2.76 eV and percentage differences to the experimental value are 9.67 and 10.39%.

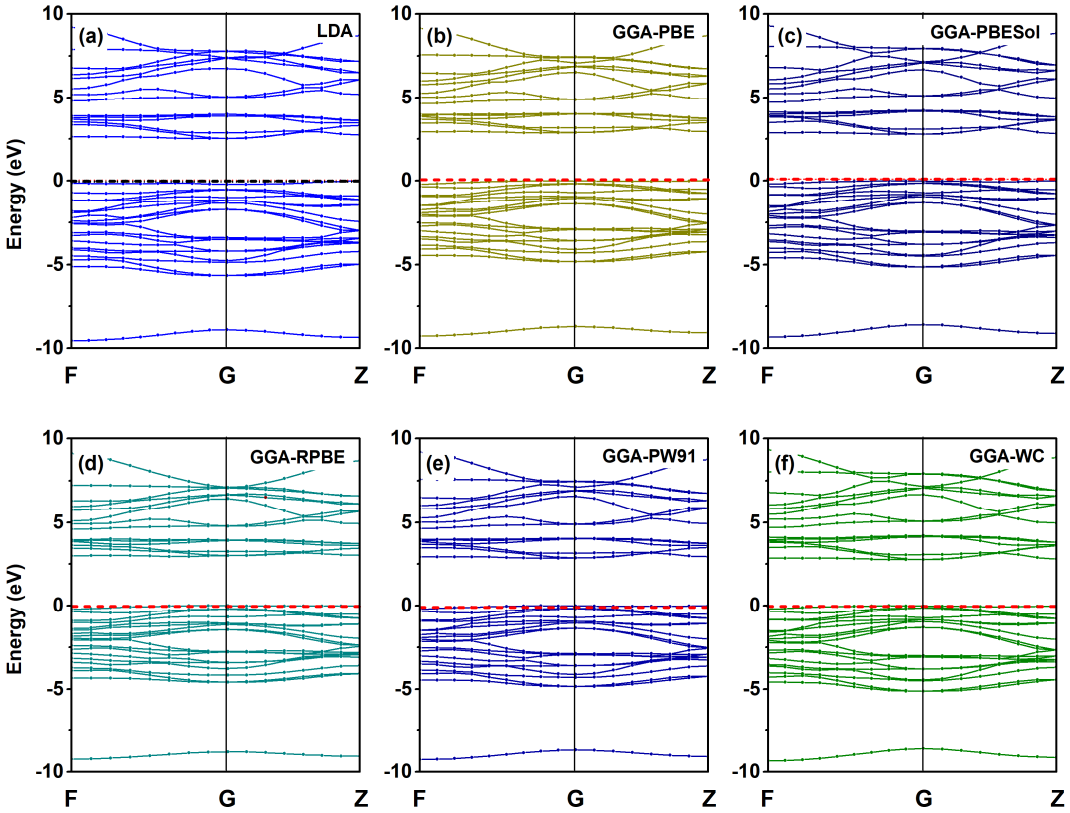

Figure 5. Band structures of BNT calculated using (a) LDA, (b) GGA-PBE, (c) GGA-PBESol, (d) GGA-RPBE, (e) GGA-PW91 and (f) GGA-WC.

Table 2. Electronic bandgaps of BNT calculated using different functionals.

Functionals	**LDA**	**PBE**	**PBESol**	**RPBE**	**PW91**	**WC**	**Exp [4].**
Bandgap (eV)	2.52	2.86	2.78	2.95	2.84	2.76	3.08
Error (%)	18.15	7.17	9.67	4.35	7.66	10.39	0

Figure 6 presents the partial density of states (PDOSs) of BNT calcualted using different functionals; the vertical dotted lines represents for Fermi level with energy of 0 eV. All calculations shows that the Fermi level lies just at the top of conduction bands, suggesting that BNT is a p-type semiconductors. The conduction bands are mainly composed of Bi-6p, Ti-3d and O-2p states while the valence band are hybridised from Ti-3d and O-2p states, in a good agreement with previous studies [42, 43]. The clearly peak at -10 eV is dominated by the hybridisation of Bi-6s and O-2p states. No clearly differences can be found between the PDOSs of BNT calculated from different functionals, except for the bandgap values.

The electronic structure obtained from all exchange-correlation functionals is consistent with the rhombohedral R3c crystal symmetry. In this phase, antiphase rotations of TiO_6 octahedra together with the off-center displacement of Ti and Bi ions modify the Ti–O–Ti bond angles and strengthen the hybridization between O-2p, Ti-3d and Bi-6p orbitals. Consequently, the valence-band maximum is dominated by O-2p states hybridized with Ti-3d orbitals, whereas the conduction-band minimum mainly originates from Ti-3d and Bi-6p states. Small variations in lattice constants predicted by different

functionals slightly alter these orbital interactions, leading to the observed differences in the calculated band gaps.

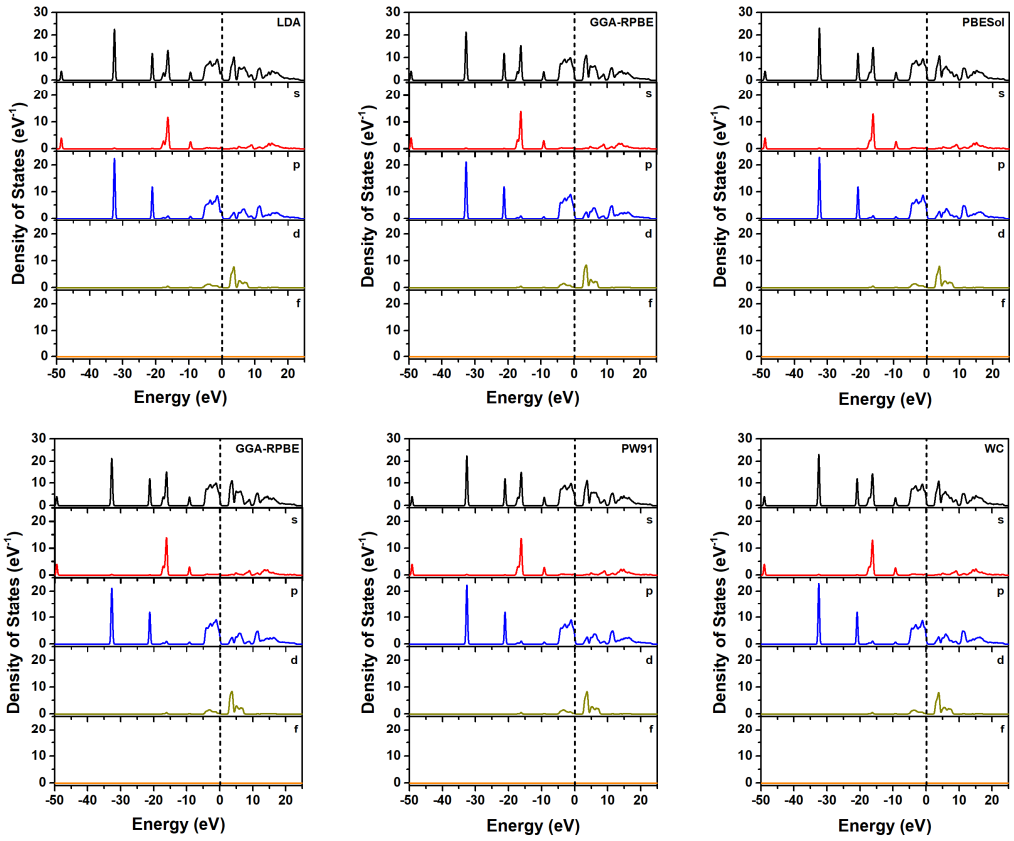

Figure 6. Projected Density of States (PDOSs) of BNT calculated using (a) LDA, (b) GGA-PBE, (c) GGA-PBESol, (d) GGA-RPBE, (e) GGA-PW91 and (f) GGA-WC.

It is worth noting that Bismuth is a heavy element (Z = 83) where relativistic effects, particularly Spin-Orbit Coupling (SOC), play a non-negligible role in the electronic band structure. The inclusion of SOC primarily affects the conduction band minimum (CBM), which is predominantly composed of Bi-6p orbitals. SOC splits the Bi-6p triplet states into j = 1/2 and j = 3/2 total angular momentum sub-states, effectively shifting the lower conduction band downward by approximately 0.2 - 0.3eV. Consequently, standard semi-local GGA functionals without SOC yield slightly larger Kohn-Sham electronic gaps that artificially appear closer to the experimental optical gap (3.08eV). When SOC is taken into account, the intrinsic functional bandgap underestimation becomes more pronounced, underscoring the necessity of higher-level approximations such as HSE06 hybrid functionals or GW quasiparticle corrections for quantitative optical alignment.

Figure 7 demonstrates the spin-resolved density of states and spin density of states of BNT obtained with different functionals. The black lines represents for states with spin-up electrons while the red lines shows the contribution of spin-down states; and the blue lines illustrates for the spin density of states of BNT. It can be seen that all the spin-resolved densities of states are symmetric, suggesting that BNT is a non-magnetic materials. However, the non-zero spin densities of states calculated using PBE, RPBE and PW91 indicates that BNT exhibit very small residual spin polarization. The calculated spin polarization is extremely small and may originate from numerical effects, including finite k-point sampling, convergence

thresholds, or small asymmetries introduced during self-consistent iterations. Since the spin-up and spin-down densities of states remain nearly symmetric and no finite magnetic moment is obtained, the present calculations do not provide sufficient evidence to conclude intrinsic magnetism in pristine BNT. Therefore, rhombohedral BNT should be regarded as essentially non-magnetic, in agreement with experimental observations. Figure 8 depicts the detailed spin densities of states of BNT, illutrating the contribution of valence electrons on the magnetic properties of material.

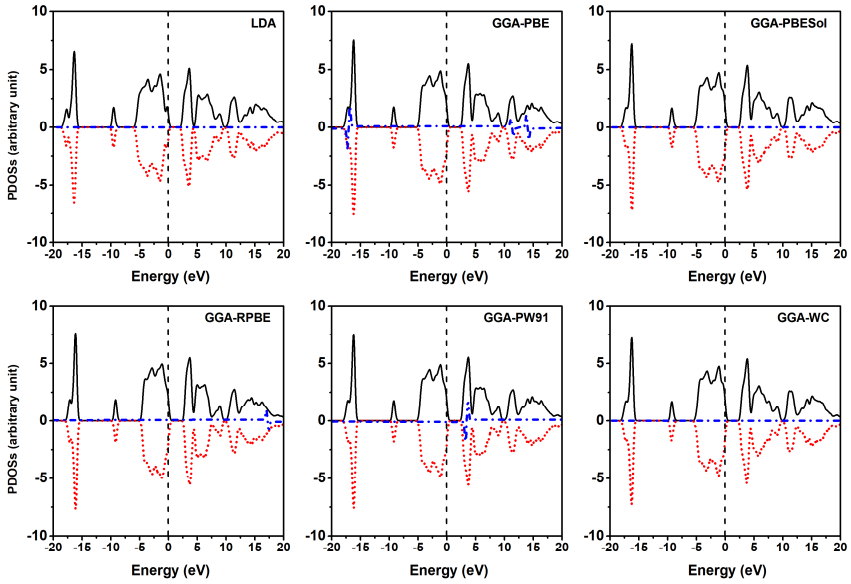

Figure 7. Spin-resolved and spin density of states of BNT calculated using (a) LDA, (b) GGA-PBE, (c) GGA-PBESol, (d) GGA-RPBE, (e) GGA-PW91 and (f) GGA-WC.

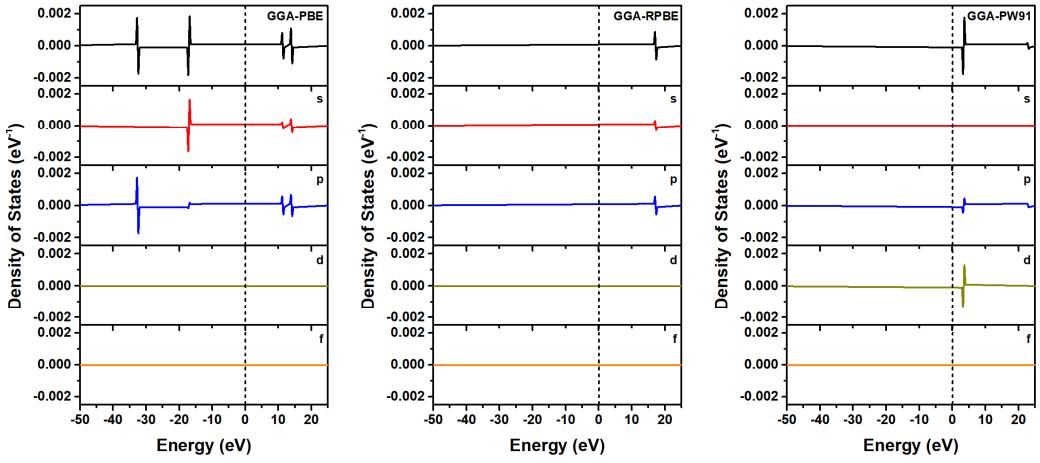

Figure 8. Spin densities of states of BNT calculated using (a) GGA-PBE, (b) GGA-RPBE and (c) GGA-PW91.

The optical bandgap of BNT can be determined from calculated absorption spectra using Wood-Tauc method [44, 45], which is applicable for both direct and indirect transitions. It is known that absorption coeficient α and bandgap value E_g are related via the equation $(\alpha h\nu)^n = A(h\nu - E_g)$, whereas A and n are constants, ν is the frequency of light and h is the Planck constant. The corresponding value of n are 2 and 1/2 for direct and indirect allowed transitions, respectively.

Figure 9 shows the Wood-Tauc plots for direct transitions in absorption spectra of BNT calculated using various functionals in the range of photon energies of 0 to 5 eV. The absorbance in the range of 0 to 2 eV is small, suggesting that BNT is tranparent for the light in that range. The absorbance increase when the photon energy is higher than about 2 eV, showing a clearly absorption edge in that range. The optical bandgaps of BNT determined from obsorption spectra are listed in Table 3. The LDA give the smallest optical bandgap of 2.51 eV while the remained functionals produced similar bandgap around 2.74 to 2.76 eV. Due to the experimental value of 3.08 eV, LDA is not reliable for bandgap estimation compared with the other functionals.

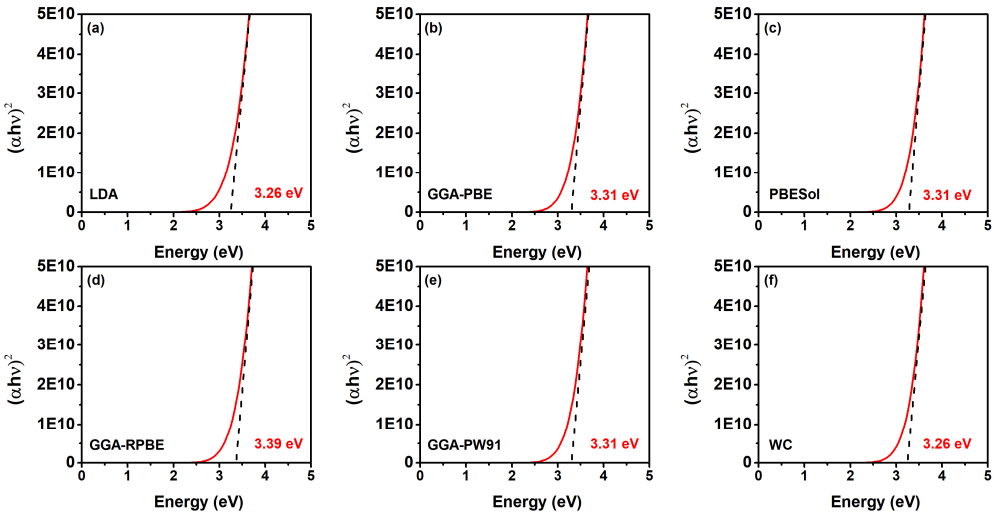

Figure 9. Wood-Tauc plots for direct transitions of absorption spectra of BNT calculated using (a) LDA, (b) GGA-PBE, (c) GGA-PBESol, (d) GGA-RPBE, (e) GGA-PW91 and (f) GGA-WC.

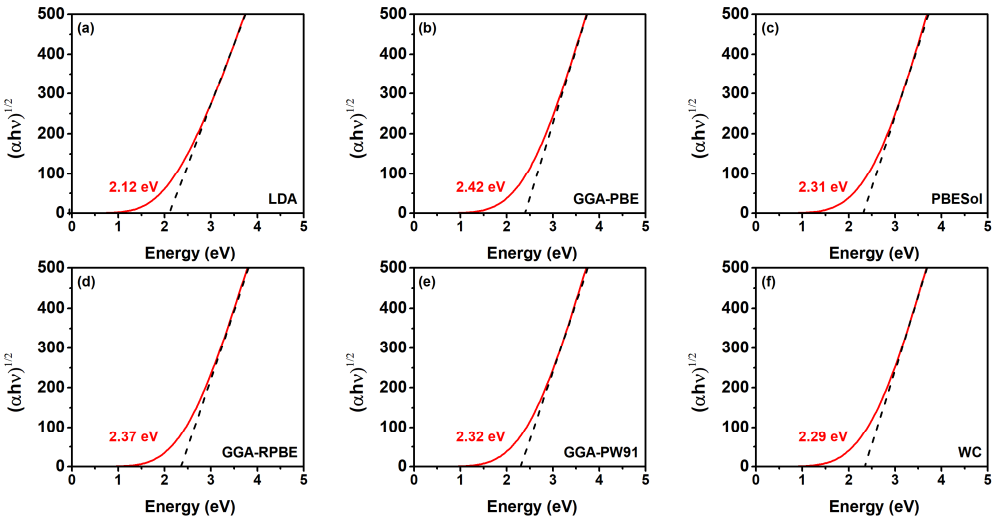

Figure 10. Wood-Tauc plots for indirect transitions of absorption spectra of BNT calculated using (a) LDA, (b) GGA-PBE, (c) GGA-PBESol, (d) GGA-RPBE, (e) GGA-PW91 and (f) GGA-WC.

Figure 10 compares the optical band gaps of BNT obtained using six different exchange-correlation functionals from the Wood–Tauc analysis. Similar to the absorption spectra presented in Figure 9, all functionals predict a direct optical transition with a well-defined linear region near the absorption edge, allowing reliable determination of the optical band gap. The calculated band gaps range from 2.12 to 2.42 eV, depending on the exchange-correlation functional. Among them, LDA yields the smallest optical band gap (2.12 eV), whereas GGA-PBE predicts the largest value (2.42 eV). The remaining functionals (PBEsol,

RPBE, PW91, and WC) produce intermediate values between 2.29 and 2.37 eV, indicating that the optical properties are only weakly affected by the choice of functional.

Compared with Figure 9, where the different functionals produce similar absorption spectra and nearly identical absorption edges, Figure 10 provides a quantitative comparison of the corresponding optical band gaps. Although the absorption edges appear close to each other in Figure 9, the Wood–Tauc analysis reveals measurable differences of up to 0.30 eV in the extracted band-gap values. The consistently smaller band gap predicted by LDA agrees with its well-known tendency to underestimate band gaps due to the over-delocalization of electronic states, while the GGA-based functionals provide slightly larger and mutually consistent values.

Table 3. Optical bandgaps of BNT calculated from absorption spectra.

Functionals		LDA	PBE	PBESol	RPBE	PW91	WC	Exp [4]
Bandgap (eV)	Direct	3.26	3.31	3.31	3.39	3.31	3.26	3.08
	Indirect	2.12	2.42	2.31	2.37	2.32	2.29	

The electronic band gap obtained from the band structure corresponding to the energy difference between the valence-band maximum and conduction-band minimum. In contrast, the optical band gap extracted from the Wood–Tauc analysis represents the onset of optical absorption, which is influenced by transition matrix elements, absorption coefficients, and possible excitonic effects [46]. Consequently, the optical band gap is generally smaller than the electronic band gap. Similar differences have been widely reported for oxide semiconductors [47].

The electronic band gap obtained from the band structure corresponding to the energy difference between the valence-band maximum (VBM) and conduction-band minimum (CBM). In contrast, the optical band gap extracted from the Wood–Tauc analysis represents the onset of optical absorption and is influenced by the optical transition matrix elements, absorption coefficient, and possible excitonic effects [48]. Therefore, the optical band gap is generally smaller than the electronic band gap, as observed for all exchange-correlation functionals considered in this work. Such differences between electronic and optical band gaps have been widely reported for oxide semiconductors and reflect the different physical quantities measured by band-structure and optical absorption analyses [45, 49].

Furthermore, although conventional GGA functionals are well known to underestimate Kohn–Sham electronic band gaps, the direct optical band gaps extracted from the calculated absorption spectra (3.26–3.39 eV) are slightly larger than the experimental value (3.08 eV) [48, 49]. This apparent discrepancy arises because the Wood–Tauc analysis is based on the calculated optical response rather than directly on the Kohn–Sham eigenvalues. In addition, experimental optical band gaps are often reduced by defects, oxygen vacancies, structural disorder, grain boundaries, and thermal broadening, all of which shift the absorption edge to lower photon energies. Consequently, a slightly larger calculated optical band gap does not contradict the well-known tendency of GGA to underestimate electronic band gaps [50].

Regarding the optical response, all functional calculations consistently exhibit strong absorption coefficients ($\alpha > 10^4$ cm^{-1}) in the near-ultraviolet regime ($\hbar w > 3.2$eV), driven by direct interband transitions from O-2p valence states to Ti-3d conduction states. The subtle discrepancies between the electronic band gap (E_g^{elec}) and optical absorption edge (E_g^{opt}) can also be attributed to momentum-dependent dipole matrix elements, where the transition probability near the zone center (Γ-point) dominates the experimental optical response.

Considering the lattice constants together with the electronic and optical band gaps obtained using

different exchange-correlation functionals summarized in Table 4, the GGA-PBE functional provides the most balanced overall performance for rhombohedral BNT and is therefore recommended for subsequent first-principles investigations of pristine and modified BNT materials.

Table 4. Summary of the calculated structural, electronic, and optical properties of rhombohedral $Bi_{0.5}Na_{0.5}TiO_3$ using different exchange-correlation functionals.

Properties	LDA	PBE	PBESol	RPBE	PW91	WC
Lattice constants	Poor	Good	Excellent	Fair	Excellent	Excellent
Electronic gap	Poor	Good	Moderate	Excellent	Good	Moderate
Optical gap	Poor	Good	Good	Good	Good	Good
Recommended	✗	✓✓✓	✓	✓✓	✓✓	✓

4. Conclusion

This study comprehensively evaluated the impact of six exchange-correlation functionals on the structural, electronic, and optical properties of rhombohedral BNT using density functional theory. The LDA-PZ approach consistently underestimates both lattice constants and electronic bandgaps, making it unreliable for BNT systems. PBESol and WC accurately reproduce experimental lattice parameters but provide less accurate electronic band-gap predictions than PBE and RPBE. Conversely, RPBE predicts favorable total energies and bandgaps but overestimates structural parameters. GGA-PBE and GGA-PW91 achieve a robust balance, offering reliable predictions across lattice constants, total energies, direct bandgaps, and optical absorption spectra. Consequently, GGA-PBE is identified as the optimal exchange-correlation functional for investigating the physical properties of pristine and chemically engineered BNT-based ferroelectric materials.

Funding: The authors declare that no funds, grants, or other support were received during the preparation of this manuscript.

Data Availability Statement: The data that support the findings of this study are available from the corresponding authors upon reasonable request.

Declaration of competing interest: The authors declare that they have no known competing financial interest or personal relationships that could have appeared to influence the work reported in this paper.

References

[1] G. A. Smolenskii, A. I. Agranovskaya, (1961). New ferroelectrics of complex composition. IV. Soviet Physics-Solid State, 2, 2651-2654.

[2] W. Zhu, Z.Y. Shen, W. Deng, K. Li, W. Luo, F. Song, X. Zeng, Z. Wang, Y. Li, (2024). A review: $(Bi,Na)TiO_3$ (BNT)-based energy storage ceramics. Journal of Materiomics, 10(1), 86-123. https://doi.org/10.1016/j.jmat.2023.05.002

[3] S. B. Vakhrushev, V.A. Isupov, B.E. Kvyatkovsky, N.M. Okuneva, I.P. Pronin, G.A. Smolensky, P.P. Syrnikov, (1985). Phase transitions and soft modes in sodium bismuth titanate. Ferroelectrics, 63(1), 153-160. https://doi.org/10.1080/00150198508221396

[4] G. O. Jones, P. A. Thomas, (2002). Investigation of the structure and phase transitions in the novel A-site substituted distorted perovskite compound Na(0.5)Bi(0.5)TiO(3). Acta Crystallogr B, 58(Pt2), 168-178. https://doi.org/10.1107/s0108768101020845

[5] M. Christensen, M. A. Einarsrud, T. Grande, (2017). Fabrication of Lead-Free $Bi_{0.5}Na_{0.5}TiO_3$ Thin Films by Aqueous Chemical Solution Deposition. Materials, 10(2), 213.
https://doi.org/10.3390/ma10020213

[6] S.-E. Park, S.-J. Chung, I.-T. Kim, (1996). Ferroic Phase Transitions in $(Na_{1/2}Bi_{1/2})TiO_3$ Crystals. Journal of the American Ceramic Society, 79(5), 1290-1296.
https://doi.org/10.1111/j.1151-2916.1996.tb08586.x

[7] D. D. Dung, N.H. Lam, L.T.K. Phuong, N.H. Thoan, L.H. Bac, D.T. Trang, P.V. Vinh, N.D. Quan, D.Q. Van, (2021). Optical properties of a new $(1-x)Bi_{1/2}Na_{1/2}TiO_3 + xPr_{1/2}Na_{1/2}TiO_3$ solid solution system. Materials Letters, 302, 130381. https://doi.org/10.1016/j.matlet.2021.130381

[8] Dang Duc Dung, Nguyen Hoang Thoan, Nguyen Quoc Dung, Nguyen Huu Lam, Vu Tien Lam, Pham Van Vinh, Pham Dinh Luong, Duong Quoc Van, (2022). Synthesis and Characterization of $(1-x)Bi_{1/2}Na_{1/2}TiO_{3+x}SrNiO_{3-\delta}$ Solid Solution System. Journal of Electronic Materials, 51(6), 2716-2731. https://doi.org/10.1007/s11664-022-09534-6

[9] Dang Duc Dung, Nguyen Hoang Thoan, Nguyen Huu Lam, Do Duc Tho, Vu Tien Lam, Nguyen Thi Trang, Duong Quoc Van, (2022). Optical properties of a new binary lead-free ferroelectric semiconductor $Bi_{1/2}Na_{1/2}TiO_3$–$Nd_{1/2}Na_{1/2}TiO_3$ solid solution system. Applied Physics A, 128(9), 798.
https://doi.org/10.1007/s00339-022-05910-5

[10] J. A. Dawson, H. Chen, I. Tanaka, (2015). Crystal structure, defect chemistry and oxygen ion transport of the ferroelectric perovskite, $Na_{0.5}Bi_{0.5}TiO_3$: insights from first-principles calculations. Journal of Materials Chemistry A, 3(32), 16574-16582. https://doi.org/10.1039/c5ta03705k

[11] F. Yang, M. Li, L. Li, P. Wu, E. Pradal-Velázquez, D. C. Sinclair, (2018). Defect chemistry and electrical properties of sodium bismuth titanate perovskite. Journal of Materials Chemistry A, 6(13), 5243-5254. https://doi.org/10.1039/c7ta09245h

[12] M. H. Ridzwan, M.K. Yaakob, M.F.M. Taib, A.M.M. Ali, O.H. Hassan, M.Z.A. Yahya, (2018). Structural, Electronic and Elastic Properties of rhombohedral phase $Bi_{0.5}Na_{0.5}TiO_3$ Using Density Functional Theory. International Journal of Electroactive Materials, 6, 36-41.
https://www.electroactmater.com/index.php/volume-6-2018?id=60&subid=311

[13] Nguyen Hoang Linh, Nguyen Hoang Tuan, Dang Duc Dung, Phung Quoc Bao, Bach Thanh Cong, Le Thi Hai Thanh, (2019). Alkali metal-substituted bismuth-based perovskite compounds: A DFT study. Journal of Science: Advanced Materials and Devices, 4(3), 492-498.
https://doi.org/10.1016/j.jsamd.2019.06.005

[14] H. Lü, S. Wang, X.S. Wang, (2014). The electronic properties and lattice dynamics of $(Na_{0.5}Bi_{0.5})TiO_3$: From cubic to tetragonal and rhombohedral phases. Journal of Applied Physics, 115(12), 124107. https://doi.org/10.1063/1.4869733

[15] L. Ju, et al., (2016). First-Principles Study of Magnetism in Transition Metal Doped $Na_{0.5}Bi_{0.5}TiO_3$ System. Chinese Journal of Chemical Physics, 29(4), 462-466. https://doi.org/10.1063/1674-0068/29/cjcp1602023

[16] M. Zeng, S. W. Or, H. L. W. Chan, (2010). First-principles study on the electronic and optical properties of $Na_{0.5}Bi_{0.5}TiO_3$ lead-free piezoelectric crystal. Journal of Applied Physics, 107(4), 043513.
https://doi.org/10.1063/1.3309407

[17] Chatta Wahiba, Brahim Lagoun, Lidjici Hamza, Abdelhakim Chadli, Abderahmane Cheriet, Hichem Farh, Hamadi Khemakhem, Khenchoul Salah, (2019). TB-mBJ Calculations of Structural and

Optoelectronic Properties of the Rhombohedral Phase of Bismuth Sodium Titanate ($Bi_{0.5}Na_{0.5}$)TiO_3. Solid State Phenomena, 297, 165-172. https://doi.org/10.4028/www.scientific.net/SSP.297.165

[18] D. Q. Van, L. M. Thu, Ş. Ţălu, (2026). First-principles investigation of structural, electronic and optical properties of rhombohedral $Na_{0.5}Bi_{0.5}TiO_3$. Journal of Nanomaterials and Applications, 2(1), 50-64. https://doi.org/10.65273/hhit.jna.2026.2.1.029

[19] Dang Duc Dung, Vu Tien Lam, Nguyen Huu Lam, Duong Quoc Van, Hoang Thoan Nguyen, Nguyen Hoang Linh, Nguyen Ngoc Trung, (2024). Surface ferromagnetism of lead-free ferroelectric bismuth sodium titanate materials. Communications in Physics, 34(1), 83-97. https://doi.org/10.15625/0868-3166/19184

[20] Quoc-Van Duong, Anh-Duong Nguyen, Cao-Khang Nguyen, Ngoc-Anh Nguyen Thi, Chinh-Cuong Nguyen, Duc-Dung Dang, Tien-Lam Vu, Minh-Thu Le, (2024). An ab initio calculation on the structural, electronic and magnetic properties of Ni-doped $Bi_{0.5}Na_{0.5}TiO_3$. HPU2 Journal of Science: Natural Sciences and Technology, 3(3), 10-19. https://doi.org/10.56764/hpu2.jos.2024.3.3.10-19

[21] Vu Tien Lam, Nguyen Huu Lam, Nguyen Hoang Linh, Duong Quoc Van, Dang Duc Dung, (2026). Influence of complex antisite defects in structural distortion, electrical and optical properties of $Bi_{0.5}Na_{0.5}TiO_3$(110) surface: A DFT investigation. Communications in Physics. 36 (3), 157-172 https://doi.org/10.15625/0868-3166/23659

[22] S. F. Yuk, et al., (2017). Towards an accurate description of perovskite ferroelectrics: exchange and correlation effects. Sci Rep, 7, 43482. https://doi.org/10.1038/srep43482

[23] P. Borlido, et al., (2019). Large-Scale Benchmark of Exchange-Correlation Functionals for the Determination of Electronic Band Gaps of Solids. J Chem Theory Comput, 15(9), 5069-5079. https://doi.org/10.1021/acs.jctc.9b00322

[24] Duong Quoc Van, Thoan Hoang Nguyen, Nguyen Huu Lam, Vu Tien Lam, Nguyen Ngoc Trung, Ngo Duc Quan, Dang Duc Dung, (2022). Fabrication and Optical Properties of Rare-Earth-Sm-Doped Lead-Free Ferroelectric $Bi_{0.5}Na_{0.5}TiO_3$ Materials. Proceedings of the International Conference on Advanced Mechanical Engineering, Automation, and Sustainable Development 2021 (AMAS2021), Springer International Publishing: Cham.

[25] P. Borlido, P. Borlido, J. Doumont, F. Tran, M. A. L. Marques, S. Botti, (2020). Validation of Pseudopotential Calculations for the Electronic Band Gap of Solids. J Chem Theory Comput, 16(6), 3620-3627. https://doi.org/10.1021/acs.jctc.0c00214

[26] Y. Shen, J. Cai, H.-C. Ding, X.-W. Shen, Y.-W. Fang, W.-Y. Tong, X.-G. Wan, Q. Zhao, C.-G. Duan, (2019). Role of Lone-Pairs in Driving Ferroelectricity of Perovskite Oxides: An Orbital Selective External Potential Study. Advanced Theory and Simulations, 2(6), 1900029.
https://doi.org/10.1002/adts.201900029

[27] C. Linderälv, A. Lindman, P. Erhart, (2017). A Unifying Perspective on Oxygen Vacancies in Wide Band Gap Oxides. The Journal of Physical Chemistry Letters, 9(1), 222-228.
https://doi.org/10.1021/acs.jpclett.7b03028

[28] M. D. Segall, Philip J. D. Lindan, M. J. Probert, C. J. Pickard, P. J. Hasnip, S. J. Clark, M. C. Payne, (2002). First-principles simulation: ideas, illustrations and the CASTEP code. J. Phys. Condens. Matter, 14, 2717-2744. https://doi.org/10.1088/0953-8984/14/11/301

[29] J. P. Perdew, A. Zunger, (1981). Self-interaction correction to density-functional approximations for many-electron systems. Phys. Rev. B, 23(10), 5048. https://doi.org/10.1103/PhysRevB.23.5048

[30] D. M. Ceperley, B. J. Alder, (1980). Ground State of the Electron Gas by a Stochastic Method. Physical Review Letters, 45(7), 566-569. https://doi.org/10.1103/PhysRevLett.45.566

[31] J. P. Perdew, K. Burke, M. Ernzerhof, (1996). Generalized Gradient Approximation Made Simple. Phys. Rev. Lett., 77(18), 3865. https://doi.org/10.1103/PhysRevLett.77.3865

[32] B. Hammer, L. B. Hansen, J. K. Nørskov, (1999). Improved adsorption energetics within density-functional theory using revised Perdew-Burke-Ernzerhof functionals. Physical Review B, 59(11), 7413-7421. https://doi.org/10.1103/PhysRevB.59.7413

[33] John P. Perdew, Adrienn Ruzsinszky, Gábor I. Csonka, Oleg A. Vydrov, Gustavo E. Scuseria, Lucian A. Constantin, Xiaolan Zhou, Kieron Burke, (2008). Restoring the Density-Gradient Expansion for Exchange in Solids and Surfaces. Physical Review Letters, 100(13), 136406. https://doi.org/10.1103/PhysRevLett.100.136406

[34] Y. Wang, J. P. Perdew, (1991). Correlation hole of the spin-polarized electron gas, with exact small-wave-vector and high-density scaling. Physical Review B, 44(24), 13298-13307. https://doi.org/10.1103/PhysRevB.44.13298

[35] Z. Wu, R. E. Cohen, (2006). More accurate generalized gradient approximation for solids. Phys. Rev. B, 73, 235116. https://doi.org/10.1103/PhysRevB.73.235116

[36] D. Vanderbilt, (1990). Soft self-consistent pseudopotentials in a generalized eigenvalue formalism. Physical Review B, 41(11), 7892-7895. https://doi.org/10.1103/PhysRevB.41.7892

[37] C. G. Broyden, (1970). The Convergence of a Class of Double-rank Minimization Algorithms 1. General Considerations. IMA Journal of Applied Mathematics, 6(1), 76-90. https://doi.org/10.1093/imamat/6.1.76

[38] R. Fletcher, (1970). A new approach to variable metric algorithms. The Computer Journal, 13(3), 317-322. https://doi.org/10.1093/comjnl/13.3.317

[39] D. Goldfarb, (1970). A Family of Variable-Metric Methods Derived by Variational Means. Mathematics of Computation, 24(109), 23-26. https://doi.org/10.1090/S0025-5718-1970-0258249-6

[40] D. F. Shanno, (1970). Conditioning of Quasi-Newton Methods for Function Minimization. Mathematics of Computation, 24(111), 647-656. https://doi.org/10.2307/2004840

[41] H. J. Monkhorst, J. D. Pack, (1976). Special points for Brillouin-zone integrations. Phys. Rev. B, 13(12), 5188. https://doi.org/10.1103/PhysRevB.13.5188

[42] D. D. Dung, N. H. Thoan, N. Q. Dung, P. V. Vinh, N. H. Lam, V. T. Lam, P. D. Luong, D. Q. Van, (2022). Magnetic Properties of a $(1-x)Bi_{0.5}Na_{0.5}TiO_3+xCaNiO_{3-\delta}$ Solid Solution System Prepared by Sol–Gel Technique. Journal of Electronic Materials, 51(5), 1905-1921. https://doi.org/10.1007/s11664-022-09457-2

[43] Dang Duc Dung, Nguyen Hoang Thoan, Nguyen Quoc Dung, Nguyen Huu Lam, Pham Van Vinh, Vu Tien Lam, Pham Dinh Luong, Duong Quoc Van, (2022). Structural, optical, and magnetic properties of a new complex $(1-x)Bi_{1/2}Na_{1/2}TiO_3 + xMgNiO_{3-\delta}$ solid solution system. Applied Physics A, 128(2), 129. https://doi.org/10.1007/s00339-021-05255-5

[44] D. L. Wood, J. Tauc, (1972). Weak Absorption Tails in Amorphous Semiconductors. Physical Review B, 5(8), 3144-3151. https://doi.org/10.1103/PhysRevB.5.3144

[45] B. Kharroubi, M. Bousmaha, R. Naceur, (2022). Combination of optical properties acquired by first principles calculations with the empirical Tauc method for determining the band gap energy of alkaline-

earth metal oxides: MO (M = Be, Mg, Ca, Sr, Ba). Journal of Computational Methods in Sciences and Engineering, 22(3), 1013-1022. https://doi.org/10.3233/JCM-220001

[46] A. Diebold, T. Hofmann, (2021). Excitons and Excitonic Effects During Optical Transitions. Optical and Electrical Properties of Nanoscale Materials, Springer International Publishing: Cham, 149-177. https://doi.org/10.1007/978-3-030-80323-0_5

[47] H.-X. Zhong, S. Gao, J.-J. Shi, L. Yang, (2015). Quasiparticle band gaps, excitonic effects, and anisotropic optical properties of the monolayer distorted 1T diamond-chain structures ReS_2 and $ReSe_2$. Physical Review B, 92(11), 115438. https://doi.org/10.1103/PhysRevB.92.115438

[48] D. D. Dung, N. T. Hung, D. Odkhuu, (2019). Magnetic and optical properties of $MgMnO_{3-\delta}$-modified $Bi_{0.5}Na_{0.5}TiO_3$ materials. Journal of Magnetism and Magnetic Materials, 482, 31-37. https://doi.org/10.1016/j.jmmm.2019.03.029

[49] M. Zeng, S. W. Or, H. L. W. Chan, (2010). First-principles study on the electronic and optical properties of $Na_{0.5}Bi_{0.5}TiO_3$ lead-free piezoelectric crystal. Journal of Applied Physics, 107(4), 043513. https://doi.org/10.1063/1.3309407

[50] M. Sharma, M. Sierka, (2024). Optical Gaps of Ionic Materials from GW/BSE-in-DFT and CC2-in-DFT. Journal of Chemical Theory and Computation, 20(21), 9592-9605. https://doi.org/10.1021/acs.jctc.4c00819